Final aspect of the accelerometer is presented in fig. 5.33a. Picture in fig. 5.33b shows the device in the optical bench. In this case, the device is under 1g acceleration, since it suffers from the earth gravitational field. It can be seen that input and output fiber optics are extremely close to the accelerometer, but still can move freely. This is an important drawback on the device characterization since a change of power at the output could be caused either by the mass movement or to a fiber misalignment. In order to assure the appropriate device characterization, fiber optics should move together with the accelerometer. This is achieved by placing them in V-grooves specially designed for this purpose.

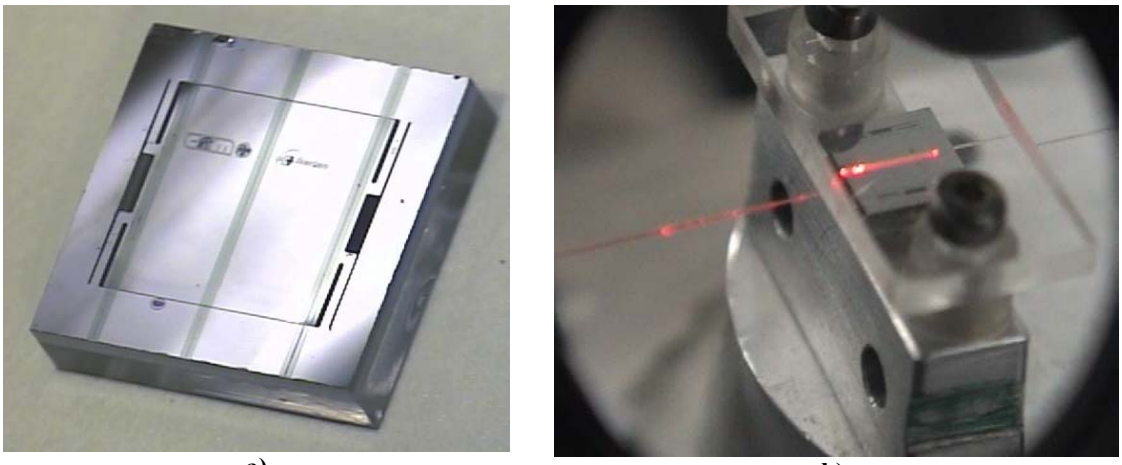

a) **b)**

Fig 5.33: Final accelerometer aspect and first measurements with fiber optics.

The V-groove fabrication can be seen in table 5.22, Process was identical as these presented in the absorption sensor, except for the fact that wafer are double-side polished. In this substrate a 0.2μm thermal oxidation and the deposition of 0.1μm LPCVD silicon nitride is also done. This latter is removed from the backside and windows are opened with RIE (for the Si_3N_4) and with wet etching (for SiO_2). A glass wafer is bonded at the backside and finally, silicon wafer is etched, though the windows, until a depth of 300μm. Wafer is cut and fiber optics are stacked at the chips. Then, chips are polished so as to have the end of the fiber at the end of the V-groove.

<table>
<tr><td>V-grooves</td><td></td></tr>
<tr><td> 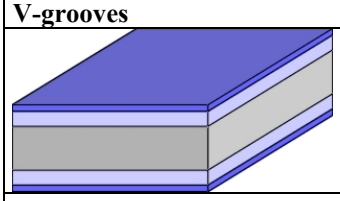 </td><td>Silicon substrate. Double-side polished, 4’ diameter, 400µm thick, N-type
0.2µm thermal SiO_2 wet growth
0.1µm LPCVD Si_3N_4 deposition</td></tr>
<tr><td> 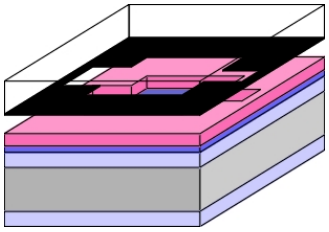 </td><td>CNM-119: Opening of the windows in silicon nitride
 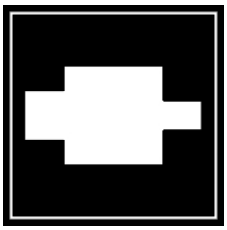
Mask:
Input width: 125µm
Output width: 4µm
Steps:
Si_3N_4 RIE back-etching with SF_6+He
2µm positive photoresist
Window definition in the Si_3N_4 with RIE using
SiO_2 wet etching (HF 49%) though the silicon nitride window</td></tr>
<tr><td> 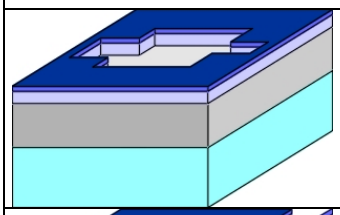 </td><td>Anodic bonding of a glass wafer at the back of the silicon wafer</td></tr>
<tr><td> 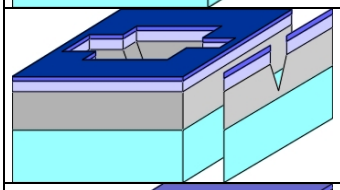 </td><td>TMAH silicon etching. 300µm</td></tr>
<tr><td> 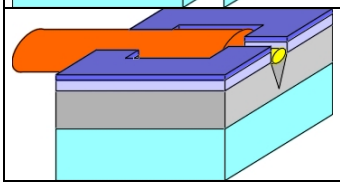 </td><td>Wafer cutting with a diamond blade
Fiber optics fixation with glue.
Polishing with SIC (0.9µm)+ Al_2O_3 (0.3µm)</td></tr>
</table>

Table 5.22: Glass wafer mechanization by anodic bonding and silicon mask.

Once V-grooves were obtained, problem arise from the fact that it is necessary to align the fiber optics in the V-groove with the input waveguide of the accelerometer before stacking them. Between the several attempts tried, the one that provides with best results is shown in table 5.23. The accelerometer is firstly fixed to a mechanized aluminium piece that has a slight minor length than the accelerometers. V-grooves are correctly aligned and stacked. When the glue has dried, two self-aligned pieces are placed underneath the V-grooves so as to provide the whole structure with stiffness.

Accelerometer pre-packaging	
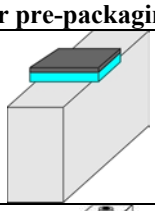	Stacking of the accelerometer to a mechanized aluminium support, being its dimensions slightly smaller than these of the device
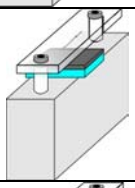	Protection with a rigid transparent plastic (methacrilate) in order to avoid damage
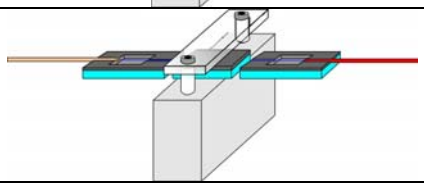	Alignment and stacking of the polished V-grooves with the optical fibers.
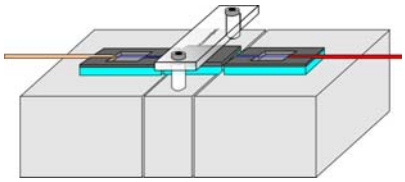	Robustness enhanced by two self-aligned aluminium pieces placed underneath the V-grooves 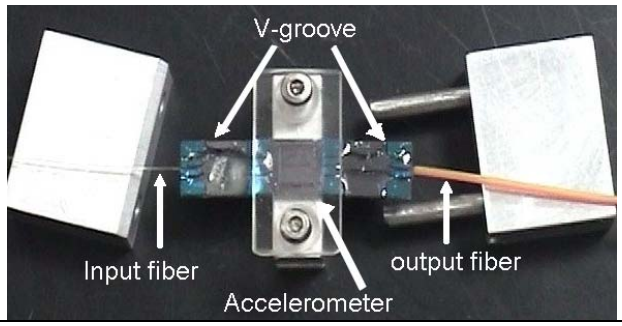

Table 5.23: V-groove and accelerometer pre-packaging steps.

First experimental results were focused on analyzing the power losses due to the different alignment processes. Reference power laser and power obtained at the end of the accelerometer was measured to be 41.5µW and 51nW, respectively, that is, the device has losses of 29dB. When V-grooves were aligned to the accelerometer, losses even had a more dramatic value, since they increased until 35.1dB. However, after stacking both structures with the appropriate glue, they were lowered to 18.3dB.

Several considerations can be done in order to justify this high attenuation. Firstly, and perhaps the most important, is the polishing step. Although it has been successfully used for the measurement of all previously described devices, the fact that both accelerometers and V-grooves have a glass wafer underneath causes polishing to be extremely difficult. Thus, the same accuracy as probably would not be obtained.

Moreover, during the polishing step, wax was used to appropriately fix the accelerometer. It has been observed that this wax reacts with the photoresist, forming a polymeric structure not only over the waveguides, but also on its faces. Although the properties of this polymer are unknown, it surely causes an increase of the losses due to scattering.

Although the device has high losses, it was still possible to do its characterization. For this purpose it was used the experimental setup shown in fig. 5.34. It consists on a Ferris wheel that has a controlled movement in such a way that the acceleration applied to the device is the projection of this magnitude to the sensible axis of the device. It can be observed that photodetector and laser source are also fixed to the mobile part of the setup. This has been done due to the fact that if they are placed outside the Ferris wheel, fiber optics would be progressively rotated and twisted, this, in turn, would cause changes in the light polarization that would mean an increase of the losses in the fiber optics.

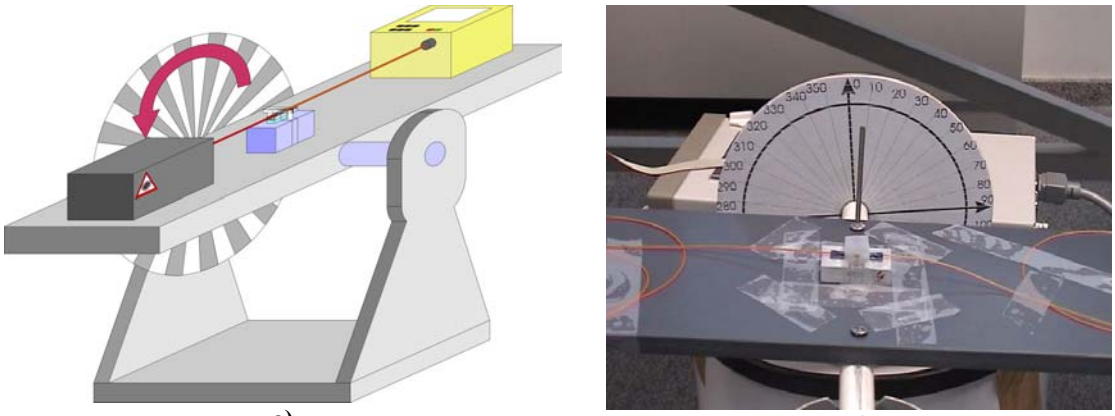

a) b)

Fig 5.34: a) Experimental setup for static accelerometer configuration, whicht consist on the light source, the photodetector and the accelerometer on a calibrated Ferris wheel. b) Detailed picture of the accelerometer positioning and fiber optics fixing on the setup.

The expected periodical response of the total losses as a function of the angle is shown in fig. 5.35. It has to be noted that losses shown in this figure have been re-ranged, being the zero fixed for the maximum power output. This has been done so as to determine the device sensitivity and to analyze if the accelerometer response was the expected. From this figure several considerations have to be taken into account. Firstly, it can be observed that minimum losses are not obtained at 90º and 270º, corresponding

to an acceleration of 0g, but have a slight displacement to 100º and 260º. This value corresponds to a misalignment between waveguides of 0.18μm.

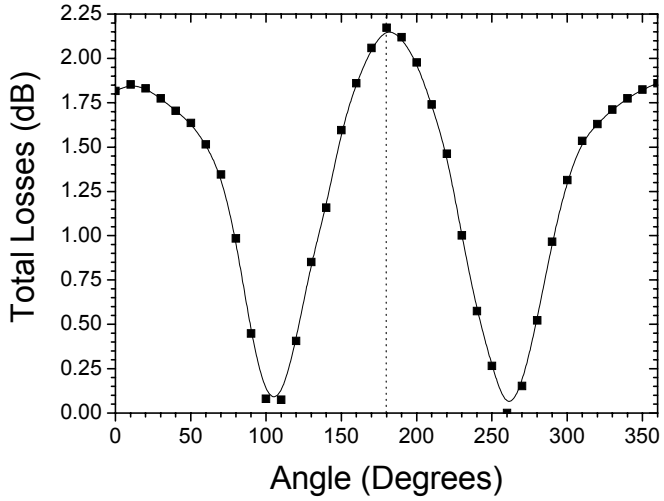

Fig. 5.35: Accelerometer output intensity as function of the gravitational field tilt.

Although the behaviour between the two minimum losses presents a very high linearity, it can be observed that seismic mass displacement does not cause symmetrical power variations, since at the region between 0 and 90º (and also between 270º and 360º) a tail is observed in the experimental data. This fact could be understood if it is taken into account that waveguides have passivation. When the accelerometer suffers from large negative values of the acceleration, light is partially injected to the passivation, causing a decrease of the losses. This fact is not observed at positive acceleration values since the silicon of the seismic mass fastly absorbs the light injected in the 2nd cladding.

Comparison between the experimental and simulation data as a function of the applied gravitational field is presented in fig. 5.36. As can be seen, there exists a significant similarity between both data, although experimental results have half of the expected sensitivity. This fact has been associated to an offset caused by the light not injected into the input waveguide at the junction between the accelerometer and the V-groove. This offset should be much lower as compared to the expected experimental results. However, due to the high insertion losses, it has been observed that have a significant effect on the final response of the device.

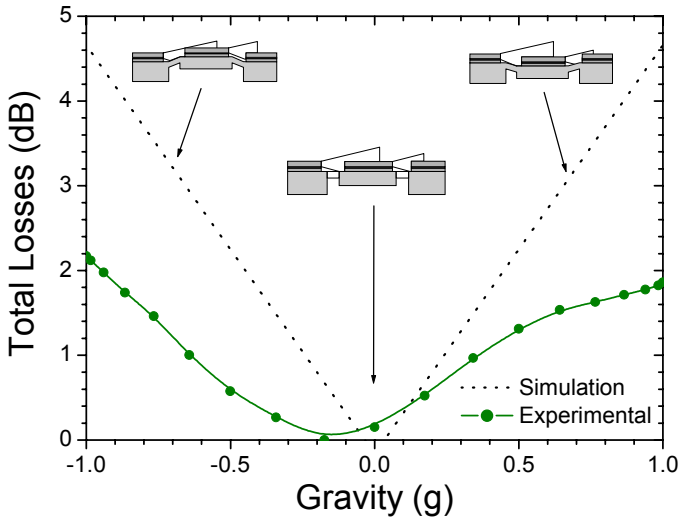

Fig. 5.36: Accelerometer output intensity as function of the gravitational field intensity.

Finally, the accelerometer response as a function of a time-dependent excitation, that is, its dynamical property was also studied. For this purpose it was used the experimental setup shown in fig. 5.37a. It basically consists on a laser source, the pre-packaged accelerometer placed on a piezoelectric which, in turn, is connected to a signal generator. The output fiber optics is directly connected to digital oscilloscope with optical readout. Results are shown in fig 5.37b. As can be seen, for frequencies far from resonance, when a trigonometric signal is applied to the piezoelectric, a frequency doubling is observed in the accelerometer response. This fact is clearly understood if it is taken into account that, due to its configuration, it cannot distinguish between positive and negative acceleration values. Thus, in each period, it crosses twice the power region where maximum power transmission is obtained. When comparing the height of both peaks, it can be observed that its high is slightly different, which again is consistent with the results obtained when studying the static response, since the passivation causes a reduction of the losses.

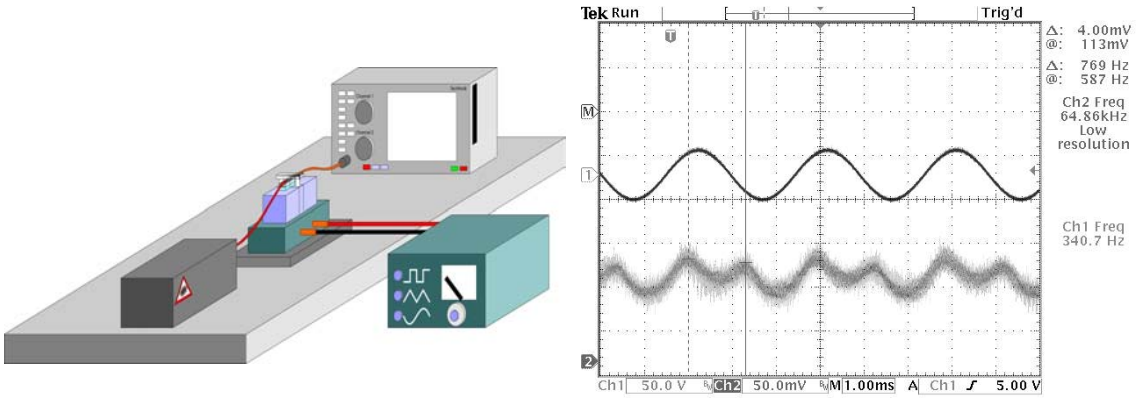

a) **b)**

Fig. 5.37: a) Experimental setup scheme for measuring the accelerometer dynamical response. b) Accelerometer output intensity when applied a time-dependent periodical signal to the piezoelectric

During this chapter several devices have been measured and compared with the simulations. Starting from the simplest structure, the waveguide, and according to its characterization, it has been possible to develop each time more complex and applicable integrated optics devices. Moreover, it has been observed that the new devices proposed in order to overcome the inherent problems of the existing devices, as could be Y-junctions or monomode waveguides, show the response predicted in the simulations and thus they can be implemented in further devices. Uniaxial optical accelerometers, the most complicated structure presented in this chapter, has many drawbacks, especially in the diaphragm configuration. However, it has been possible to do an accurate characterization of the misalignment accelerometer. Experimental results of the presented uniaxial misalignment accelerometer show that, although asymmetrical, total losses present a wide linear region as a function of the gravitational field. So far, main problems are due to the significant offset and to the high insertion losses due to inappropriate facet polishing.

Bibliography

[1] I.Garcés. Estudio *Teórico y Desarrollo Experimental de Guías de Onda Ópticas en Tecnología de Silicio: Aplicación al Diseño de Sensores Optoquímicos*. Thesis. Universidad de Zargoza. 1996

[2] David Jiménez Jiménez. *Diseño de Dispositivos Optoelectrónicos Integrados: Métodos Numéricos de Simulación de la Propagación de Ondas Electromagnéticas*.Thesis. Universitat Autònoma de Barcelona 2000.

[3] F.Prieto. *Sensores Interferométricos Mach-Zehnder Integrados Basados en Guías de Onda ARROW para Aplicaciones Biosensoras*, Thesis. 2002. Universidad Autónoma de Madrid.

[4] K.Tiefenthaler, W.Lucosz. *Sensitivity of Grating Couplers as Integrated-Optical Chemical Sensors*. J.Opt.Soc.Am.B 6, 209-220. 1989.

[5] E.F.Shipper, A.M.Brugman, C.Domínguez, L.M.Lechuga, R.P.H.Kooyman, J.Greve. *The Realisation of an Integrated Mach-Zehnder Waveguide Immunosensor in Silicon Technology.* Sens.& Act.B 40, 147-153. 1997.

[6] I.Salinas. (Title to be confirmed), Thesis. Universidad de Zaragoza. 2002

[7] M.Puyol. *Sensores optoquímicos integrados basados en guías de onda*, Thesis. Universitat Autònoma de Barcelona. 2002

[8] J.A.Plaza, A.Llobera, J.Esteve, C.Domínguez, J.Berganzo, J.García. *Acelerómetro Óptico Integrado*. Patent num. 200200854. Spain 2002.